



1 **Large-scale sensitivities of groundwater and surface water to**
2 **groundwater withdrawal**

3
4 *Marc F.P. Bierkens^{1,2,#}, Edwin H. Sutanudjaja¹ and Niko Wanders¹*

5
6 ¹Department of Physical Geography, Utrecht University, P.O. Box 80115, 3508 TC Utrecht,
7 The Netherlands

8 ²Unit Soil and Groundwater Systems, Deltares, P.O. Box 85467, 3508 AL Utrecht, The
9 Netherlands

10 # Correspondence to: m.f.p.bierkens@uu.nl

11

12

13 **Abstract**

14 Increasing population, economic growth and changes in diet have dramatically increased the
15 demand for food and water over the last decades. To meet increasing demands, irrigated
16 agriculture has expanded into semi-arid areas with limited precipitation and surface water
17 availability. This has greatly intensified the dependence of irrigated crops on groundwater
18 withdrawal and caused a steady increase of non-renewable groundwater use, i.e. groundwater
19 taken out of aquifer storage that will not be replenished in human time scales. One of the
20 effects of groundwater pumping is the reduction in streamflow through capture of
21 groundwater recharge, with detrimental effects on aquatic ecosystems. The degree to which
22 groundwater withdrawal affects streamflow or groundwater storage depends on the nature of
23 the groundwater-surface water interaction (GWSI). So far, analytical solutions that have been
24 derived to calculate the impact of groundwater on streamflow depletion involve single wells
25 and streams and do not allow the GWSI to shift from connected to disconnected, i.e. from a
26 situation with two-way interaction to one with a one-way interaction between groundwater
27 and surface water. Including this shift and also analyse the effects of many wells, requires
28 numerical groundwater models that are expensive to setup. Here, we introduce a simple
29 conceptual analytical framework that allows to estimate to what extent groundwater
30 withdrawal affects groundwater heads and streamflow. It allows for a shift in GWSI,
31 calculates at which critical withdrawal rate such a shift is expected and when it is likely to
32 occur after withdrawal commences. It also provides estimates of streamflow depletion and
33 which part of the groundwater withdrawal comes out of groundwater storage and which parts
34 from a reduction in streamflow. After a local sensitivity analysis, the framework is used to
35 provide global maps of critical withdrawal rates and timing, the areas where current
36 withdrawal exceeds critical limits, and maps of groundwater depletion and streamflow
37 depletion rates that result from groundwater withdrawal. The resulting global depletion rates



38 are similar to those obtained from global hydrological models and satellites. The analytical
39 framework is particularly useful for performing first-order sensitivity studies and for
40 supporting hydroeconomic models that require simple relationships between groundwater
41 withdrawal rates and the evolution of pumping costs and environmental externalities.

42

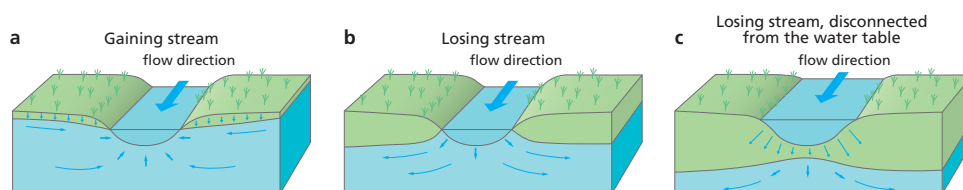
43 **1. Introduction**

44 Increasing population, economic growth and changes in diet have dramatically increased the
45 demand for food and water over the last decades (Godfray et al., 2010). To meet increasing
46 demands, irrigated agriculture has expanded into semi-arid areas with limited precipitation
47 and surface water (Siebert et al., 2015). This has greatly intensified the dependence of
48 irrigated crops on groundwater withdrawal (Wada et al., 2012) and caused a steady increase
49 of non-renewable groundwater use, i.e. groundwater taken out of aquifer storage that will not
50 be replenished in human time scales (Wada and Bierkens, 2019). Recent estimates of current
51 groundwater withdrawal range approximately between 600-1000 m³ yr⁻¹ and consumptive
52 use of non-renewable groundwater between 150-400 m³ yr⁻¹ (Wada, 2016).

53

54 Groundwater that is pumped comes either out of storage, from reduced groundwater
55 discharge or from reduction of surface evaporation fed from below by groundwater through
56 capillary rise and/or phreatophytes (Theis, 1940; Alley et al. 1999; Bredehoeft, 2002);
57 Konikow and Leake, 2014). Thus, extensive groundwater pumping not only leads to
58 groundwater depletion (Wada et al., 2010) but also to a reduction in streamflow (Wada et al.,
59 2013; Mukherjee et al., 2019; De Graaf et al., 2019) and desiccation of wetlands and
60 groundwater dependent terrestrial ecosystems (Runhaar et al 1997; Shafroth et al., 2000;
61 Elmore et al 2006; Yin et al 2018). However, the effect of groundwater pumping on
62 groundwater depletion and surface water depletion heavily depends on the nature of the
63 interaction between groundwater and surface water. Limiting ourselves to phreatic
64 groundwater systems and following Winter et al. (1998), a distinction can be made between
65 gaining streams, losing streams and disconnected losing streams, depending on the position
66 of the free groundwater surface with respect to the surface water level and the bottom of the
67 stream (Figure 1). Since groundwater pumping affects groundwater levels, it can move a
68 stream from gaining to losing to disconnected and losing, which, in turn, affects the way
69 that groundwater pumping affects streamflow.

70



71
72 *Fig. 1. Groundwater-streamflow interaction: (a) gaining stream; (b) losing stream; (c) losing*
73 *stream disconnected from the water table; modified from Winter et al. (1998); credit to the*
74 *United States Geological Survey.*
75

76 Based on the above, Bierkens and Wada (2019) define two stages of groundwater withdrawal
77 in phreatic aquifers. In stage 1, groundwater withdrawal is such that the water table remains
78 connected with the surface water system (Figure 1a, b). Upon pumping, groundwater initially
79 comes out of storage and groundwater levels decline. However, as groundwater levels decline
80 around a well, the well attracts more of the recharge that would otherwise end up in the
81 stream until a new equilibrium is reached where all of the pumped water comes out of
82 captured streamflow. In a stage 1 withdrawal regime, withdrawal is said to be physically
83 sustainable in that groundwater depletion is limited and groundwater withdrawal mostly
84 diminishes streamflow and evaporation. Depending on the groundwater level, one could
85 further distinguish between gaining (Figure 1a) and losing (Figure 1b) streams. This is
86 important when considering the quality of pumped groundwater as in case of a losing stream
87 surface water ends up in the well. In a stage 2 withdrawal regime, groundwater withdrawal is
88 so large that groundwater levels fall below the bottom of the stream (Figure 1c). In that case,
89 a further decline of the groundwater level hardly increases infiltration from the stream to the
90 aquifer. Thus, in stage 2, groundwater withdrawal in excess of recharge and (constant) stream
91 water infiltration is physically unsustainable and as a result leads to groundwater depletion
92 and does not impact streamflow any further even if pumping rates increase.

93
94 From the above it follows that there is a critical transition between stage 1 and stage 2
95 groundwater withdrawal that depends on groundwater withdrawal rate. In reality, this
96 transition is less abrupt. Right after the water table is just below the river bottom, negative
97 pressure heads occur below the river bed while the soil is fully or partly saturated. Wang et
98 al. (2015) show experimentally and theoretically that a full disconnection, i.e. the water table
99 has no impact on the infiltration flux, occurs only when the depth of the groundwater table
100 below the stream becomes larger than the stream water depth. Another reason is that these
101 transitions does not occur abruptly is that multiple surface water bodies in the surroundings



102 of groundwater wells differ in depth depending on stream order and location in the river
103 basin. We also note that that in many regions of the world groundwater is pumped from
104 deeper confined or leaky-confined aquifers (De Graaf et al., 2017). Under confined
105 conditions, groundwaters-streamflow interaction only occurs for the larger rivers that are
106 deep enough to penetrate the confining layer, while in leaky confined aquifers the
107 interactions are more complicated and delayed (Hunt, 2003).

108

109 There are many analytical solutions for calculating the stream depletion rate (SDR), defined
110 as the ratio of the volumetric rate of water abstraction from a stream to groundwater pumping
111 rate. These solutions differ in assumptions about the type of aquifer (unconfined, confined,
112 leaky-confined, multiple aquifers), stream bottom elevation, stream geometry and including
113 additional resistance from the streambed clogging layer or not. We refer to Huang et al.
114 (2018) for an extensive overview of solutions and when to apply them. These analytical
115 solutions typically involve a single well and a single stream, or, using apportionment
116 methods, a single well and stream networks (Zipper et al., 2019), while they consider streams
117 to be connected with the water table. For more complex situations, with multiple wells,
118 increasing withdrawal rates and streams changing from e.g. connected to disconnected,
119 numerical groundwater models need to be used. These have the disadvantage that they are
120 parameter-greedy, time-consuming to setup and often computationally expensive. Thus,
121 relatively simple generic analytical tools to assess the effects of extensive multi-well
122 groundwater pumping on groundwater and surface water systems at large are lacking.

123

124 Here, we introduce a simple conceptual analytical framework that aims to estimate for larger
125 scales, i.e. large catchments and/or regional-scale phreatic aquifer systems, to what extent
126 multi-well groundwater withdrawal affects groundwater heads and streamflow. It allows for a
127 shift in the nature of groundwater-surface water interaction, calculates at which critical
128 withdrawal rate such a shift is expected and when it is likely to occur after withdrawal
129 commences. It also provides estimates of streamflow depletion and the partitioning between
130 groundwater storage depletion and reduction in streamflow (capture). We envision that such
131 an analytical framework is particularly useful for performing first-order sensitivity studies
132 and support hydroeconomic models that require simple relationships between large-scale
133 groundwater withdrawal rates and the evolution of pumping costs and environmental
134 externalities.

135



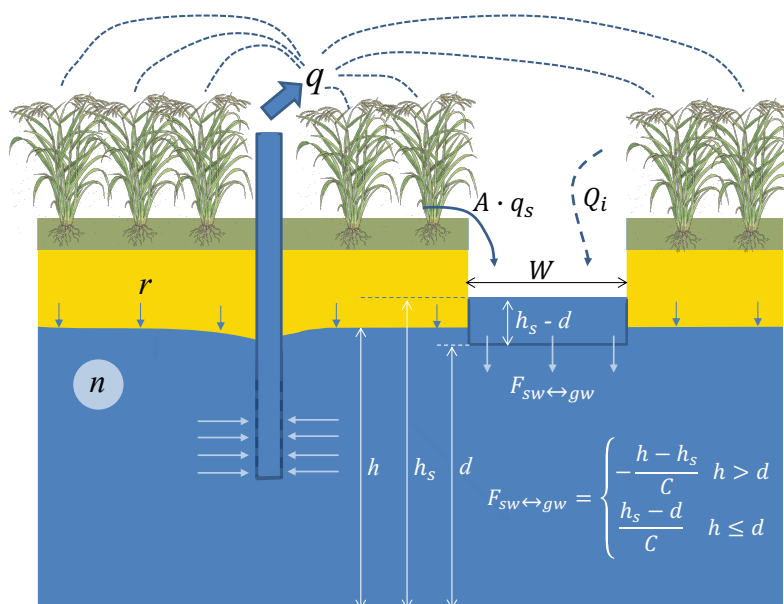
136 In the following, we first introduce the conceptual model of large-scale groundwater pumping
 137 with groundwater-surface water interaction. Next, we show its properties with an extensive
 138 sensitivity analysis, followed with a global application of the model and an evaluation of its
 139 performance with depletion estimates from satellites.

140
 141

142 **2. Conceptual model of large-scale groundwater pumping with**
 143 **groundwater-surface water interaction**

144 A conceptual hydrogeological model is proposed that allows for the analytical treatment of
 145 large-scale groundwater decline under varying pumping rates, yet exhibits the properties of
 146 surface water-groundwater interaction. Consider a simplified model of a phreatic aquifer
 147 subject to groundwater pumping (Figure 2). The volume of groundwater pumped sums up all
 148 the pumping efforts of a large number of land owners that all draw water from the same
 149 aquifer that can be seen as a common pool resource. Recharge consist of diffuse recharge
 150 from precipitation and concentrated recharge from river-bed infiltration, where river
 151 discharge comes from local surface runoff and from inflow from upstream areas outside the
 152 area of interest.

153



154
 155 *Figure 2. Conceptual model of groundwater extracted (in this case for irrigation) from an*
 156 *aquifer recharged by diffuse recharge and riverbed infiltration. Symbols are explained in the*
 157 *text.*



158 We neglect groundwater flow processes within the aquifer and the mutual influence of
159 multiple wells by treating the aquifer as one pool with a given specific yield and unknown
160 depth (i.e. physical limits are unknown) subject to pumping treated as a diffuse sink. The
161 latter is a simplification that represents the effects of thousands of wells of farmers spread
162 more or less evenly across the aquifer. Also, we assume withdrawal rate, surface runoff and
163 river bed recharge to be constant in time, neglecting seasonal variations that usually occur
164 due to variation in crop water demand. These simplifications allow us to represent the change
165 of groundwater level h with a simple linear differential equation of the total aquifer mass
166 balance:

$$167 \quad n \frac{dh}{dt} = r + F_{gw \leftrightarrow sw}(h) - q \quad (1)$$

168 With

169 h : groundwater head (m)

170 n : specific yield (-)

171 q : pumping rate per area ($\text{m}^3 \text{m}^{-2} \text{y}^{-1}$)

172 $F_{gw \leftrightarrow sw}$: surface water infiltration (or drainage) flux density ($\text{m}^3 \text{m}^{-2} \text{y}^{-1}$)

173

174 The groundwater - surface water flux is modelled as follows:

$$175 \quad F_{gw \leftrightarrow sw}(h) = \begin{cases} -\frac{h-h_s}{c} & h \geq d \\ \frac{h_s-d}{c} & h < d \end{cases} \quad (2)$$

176 with h_s is the surface water level and d the elevation of the bottom of the water course. The
177 parameter C is a drainage resistance (days) which pools together all the parameters of
178 surface-water groundwater interaction, i.e. the density or area fraction of surface waters,
179 surface water geometry and river/lake-bed conductance and the hydraulic conductivity of the
180 aquifer. Equation (2), is also used to describe groundwater-surface water interaction in
181 numerical groundwater such as MODFLOW (McDonald and Harbaugh, 2005), as well as in
182 several large-scale hydrological models (Döll et al., 2014; Sutanudjaja et al., 2018). This is a
183 simplification of the true interaction where in case of a detachment of the groundwater level
184 and the river bed ($h < d$) negative pressure heads can occur below the river bed and Equation
185 (2) may underestimate the river bed infiltration (Brunner et al., 2010). However, this study
186 also shows that errors remain within 5% in case the surface water is deep enough (> 1 m).
187 Equation (2) provides a critical transition in terms of the effect of pumping on the
188 hydrological system. As long as the groundwater level is above the bottom of the surface
189 water network, the groundwater-surface water flux acts as a negative feedback on



190 groundwater level decline, at the expense of surface water decline. As it falls below the
191 bottom elevation (only possible if pumping rate q is large enough; see hereafter), surface
192 water decline stops and progressive groundwater decline sets in.

193 The surface water level itself is a variable which is related to the surface water discharge Q
194 (m^3/day) and the groundwater level as follows:

$$195 \quad Q = Wv(h_s - d) = Q_i + q_s A + F_{gw \leftrightarrow sw}(h)A \quad (3)$$

196 with

197 A : The area over the (sub-)aquifer considered (m^2)

198 q_s : surface runoff (m y^{-1})

199 Q_i : influx of surface water from upstream ($\text{m}^3 \text{y}^{-1}$)

200 W : Stream width (m)

201 d : Bottom elevation stream (m)

202 v : Stream flow velocity (m y^{-1})

203

204 The influx Q_i is added to account for aquifers in dry climates where the surface water system
205 is fed by wetter upstream areas, e.g. mountain areas. The surface runoff q_s (including shallow
206 subsurface storm runoff) also supplements the streamflow. Equation (3) lumps the
207 streamflow system overlying the phreatic aquifer system with a representative discharge,
208 water height, flow velocity and stream width taken constant in time. Equations (1)-(3)
209 together describe the coupled surface water-groundwater system where, all parameters and
210 inputs remain constant with time and groundwater head h and surface water levels h_s change
211 over time as a result of groundwater pumping only.

212

213 In Appendix A expressions are derived for the following properties of the coupled system:

214 q_{crit} Critical pumping rate ($\text{m}^3 \text{m}^{-2} \text{y}^{-1}$) above which the groundwater level becomes
215 disconnected from the stream.

216 t_{crit} Critical time (years after start of withdrawal) at which the groundwater level
217 becomes disconnected from the stream, i.e. $h < h_s$.

218 $h(t)$ Groundwater head (m) over time

219 $h(\infty)$ Equilibrium groundwater head (m) at $t=\infty$ that only occurs in case $q \leq q_{crit}$

220 $h_s(t)$ Surface water level (m) over time.

221 $h_s(\infty)$ Equilibrium surface water level (m), which is different when $q \leq q_{crit}$ than when
222 $q > q_{crit}$.



- 223 $Q(t)$ Surface water discharge ($\text{m}^3 \text{y}^{-1}$) over time.
 224 $Q(\infty)$ Equilibrium surface water discharge ($\text{m}^3 \text{y}^{-1}$), which is different when $q \leq q_{crit}$
 225 than when $q > q_{crit}$.
 226 $q_{stor}(t)$ Part of the pumped groundwater that comes out of storage, which is different
 227 when $q \leq q_{crit}$ than when $q > q_{crit}$.
 228 $q_{cap}(t)$ Part of the pumped groundwater that comes from capture (reduction in
 229 streamflow), which is different when $q \leq q_{crit}$ than when $q > q_{crit}$.

230

231 *Table 1. Overview of derived expressions for groundwater properties used in this paper*

$\alpha = \frac{Q_i C + q_s A C + W v d C}{W v C + A}$ $\beta = \frac{A}{W v C + A}$ $q_{crit} = r + \frac{Q_i + q_s A}{W v C + A}$		
$q \leq q_{crit}$	$q > q_{crit}$	
	$t_{crit} = \frac{nC}{1-\beta} \ln \left(\frac{qC}{qC - (rC + \alpha) + d(1-\beta)} \right)$	
	$t \leq t_{crit} (h \geq d)$	$t > t_{crit} (h < d)$
$h(t) = \frac{rc + \alpha}{1-\beta} - \left(\frac{qC}{1-\beta} \right) \left[1 - e^{-\left(\frac{1-\beta}{nC}\right)t} \right]$ $h(\infty) = \frac{rc + \alpha - qC}{1-\beta}$	$h(t) = \frac{rc + \alpha}{1-\beta} - \left(\frac{qC}{1-\beta} \right) \left[1 - e^{-\left(\frac{1-\beta}{nC}\right)t} \right]$	$h(t) = d + \left[\frac{r - q}{n} + \frac{(Q_i + q_s A)}{n(W v C + A)} \right] (t - t_{crit})$
$h_s(t) = \alpha + \beta h(t)$ $h_s(\infty) = \alpha + \frac{\beta(rc + \alpha - qC)}{1-\beta}$	$h_s(t) = \alpha + \beta h(t)$	$h_s = d + \frac{(Q_i + q_s A)C}{W v C + A}$
$Q(t) = Q_i + q_s A - \frac{A\alpha}{C} + \frac{A(1-\beta)}{C} h(t)$ $Q(\infty) = Q_i + (q_s + r - q)A$	$Q(t) = Q_i + q_s A - \frac{A\alpha}{C} + \frac{A(1-\beta)}{C} h(t)$	$Q = \frac{(Q_i + q_s A)W v C}{W v C + A}$
$q_{stor} = q e^{-\left(\frac{1-\beta}{nC}\right)t}$ $q_{cap} = q \left(1 - e^{-\left(\frac{1-\beta}{nC}\right)t} \right)$	$q_{stor} = q e^{-\left(\frac{1-\beta}{nC}\right)t}$ $q_{cap} = q \left(1 - e^{-\left(\frac{1-\beta}{nC}\right)t} \right)$	$q_{stor} = q - \left(r + \frac{(Q_i + q_s A)}{(W v C + A)} \right)$ $q_{cap} = r + \frac{(Q_i + q_s A)}{(W v C + A)}$

232

233 Table 1 provides an overview of the mathematical expressions derived for each of these
 234 properties in Appendix A. The left column shows the physically sustainable regime where
 235 upon commencement of pumping after some time an equilibrium is reached with equilibrium



236 groundwater levels $h(\infty)$, streamflow $Q(\infty)$ and surface water level $h_s(\infty)$. For reasons of
 237 brevity, we will skip the term “physically” before “(non-)sustainable”, while understanding
 238 that we only refer to sustainability in the physical sense, which does not imply economic or
 239 environmental sustainability (Bierkens and Wada, 2019). The middle and right columns show
 240 the results of non-sustainable groundwater withdrawal. The behavior of $h(t)$, $Q(t)$ $h_s(t)$
 241 follows that of the sustainable regime until time $t = t_{crit}$ when the groundwater level drops
 242 below the bottom of the surface water. After this time the groundwater level $h(t)$ shows a
 243 persistent decline and surface water level $h_s(t)$, streamflow $Q(t)$ and the fraction of water
 244 pumped from capture become constant.

245

246 3. Local sensitivity analyses

247 Figure 3 shows the results of a sensitivity analysis for the critical withdrawal rate q_{crit} and the
 248 critical time until the water table disconnects from the stream t_{crit} . For the sustainable regime
 249 ($q \leq q_{crit}$) it shows the change in groundwater level at equilibrium $dh = h(0) - h(\infty)$, the change
 250 in streamflow at equilibrium $dQ = Q(0) - Q(\infty)$ and the e -folding time $t_{ef} = nC / (1 - \beta)$ of
 251 reaching the equilibrium after the commencement of pumping. For the non-sustainable
 252 regime, we show the decline rate of the groundwater level dh/dt , the (constant) streamflow
 253 depletion dQ and the constant fraction of capture ($f_{cap} = q_{cap}/q$). We stress that our sensitivity
 254 analysis is far from exhaustive (global) and that sensitivity plots are shown to provide a
 255 general feel of the behavior of the model and to show relationships between parameters and
 256 outputs that are of interesting to show. Unless they are varied on one of the axes, the
 257 parameter values used are the reference values denoted in Table 2.

258

259 *Table 2. Reference parameter values used in sensitivity analyses.*

Parameter	Value
Surface water system	
A	1000 km ²
q_s	0.001 m d ⁻¹
Q_i	50 m ³ s ⁻¹
D	95 m
W	20 m
V	1 m s ⁻¹
Hydrogeology	
C	1000 d
n	0.3
r	0.001 m d ⁻¹

260



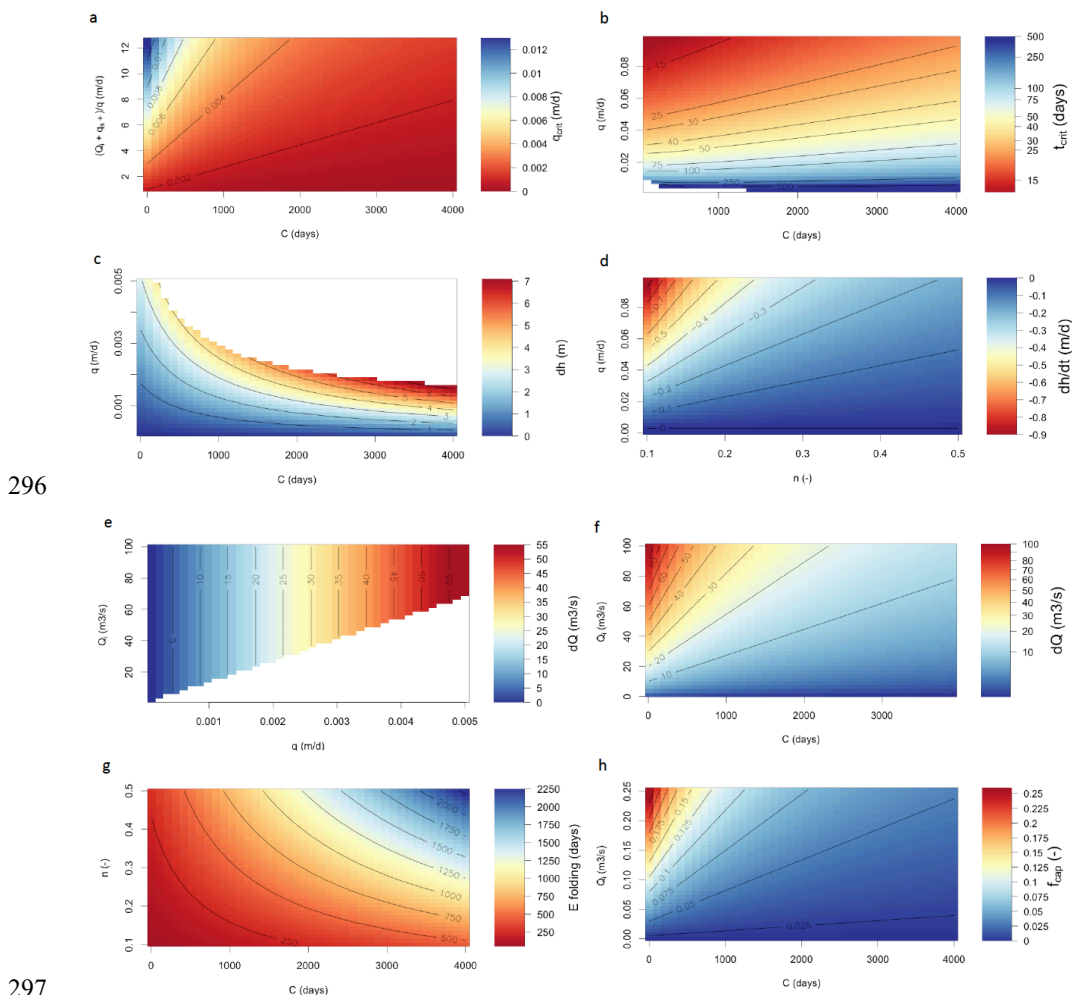
261 Figure 3a shows that the critical withdrawal rate increases with the relative abundance of
262 surface water due to upstream inflow and runoff and decreases with a decreased strength of
263 the surface water-groundwater interaction (increased value of C). For sustainable withdrawal
264 rates we see the largest equilibrium groundwater level declines with increased pumping rates
265 and decreased strength of surface water-groundwater interaction, i.e. decreased capture
266 (Figure 3c). Figure 3e shows that the equilibrium reduction in streamflow to be proportional
267 to groundwater withdrawal rate as expected, but to depend only mildly on the upstream
268 inflow. The latter is caused by the two-way interaction between surface water and
269 groundwater: increasing inflow for a given withdrawal rate reduces groundwater level
270 decline, which in turn limits the loss of surface water to the groundwater. As follows from the
271 expression $t_{ef} = nC/(1 - \beta)$, the time to equilibrium (Fig. 3g), i.e. the time until the
272 pumped groundwater originates completely from capture and no further storage changes
273 occur, is proportional to the resistance value C and the specific yield, where the degree of
274 proportionality depends on the surface water properties. Figure 3g also shows that the time to
275 full capture can be very large, up to several tenths of years.

276

277 Figures 3b-h (right column) provides sensitivity plots of relevant variables in the non-
278 sustainable regime. Figure 3b shows that under the non-sustainable regime, the time t_{crit} to a
279 transition from a connected to a non-connected groundwater table decreases with withdrawal
280 rate, but slightly increases with C . The latter seems counter-intuitive at first, because a larger
281 value of C means reduced surface water contribution and therefore likely larger groundwater
282 level decline rates and smaller values of t_{crit} . The equation for $h(t)$ in Table 1 (Equation A10
283 in the appendix) shows that this is indeed the case for early times but that for later times the
284 decline rates are reduced by a larger value of C in the term factor $(1 - \beta)/nC$ in the
285 exponential. Figures 3d-h show sensitivity plots for $t > t_{crit}$ ($h < d$), i.e. groundwater levels are
286 disconnected from the surface water, groundwater is persistently taken out of storage and the
287 capture becomes constant. As expected, the groundwater level decline rates (Figure 3d) are
288 proportional to withdrawal rates and inversely proportional to specific yield. The final
289 reduction in streamflow (Figure 3f) for $t > t_{crit}$ decreases with the value of C (limited surface
290 water-groundwater interaction), while the availability of surface water is important for
291 smaller values of C . Here, a larger inflow leads to larger losses because losses are
292 proportional to the surface water level which increases with inflow. Figure 3h resembles that



293 of Figure 3f because apart from the constant recharge, the fraction of capture is proportional
 294 to the streamflow reduction which ends up in the pumped groundwater
 295



297
 298 *Figure 3. Results of the sensitivity analyses showing parameter dependence of q_{crit} (a) and*
 299 *t_{crit} (b); variables under sustainable withdrawal: $dh=h(0)-h(\infty)$ (c), $dQ = Q(0)-Q(\infty)$ (e),*
 300 *$t_{ef} = nC/(1 - \beta)$ (g) t_{crit} and variables under non-sustainable withdrawal and $t > t_{crit}$: dh/dt*
 301 *(d), dQ (f) and $f_{cap} = q_{cap}/q$ (h).*

303 4. Global-scale application

304 We applied the analytical framework to the global scale at 5 arc-minute resolution
 305 (approximately 10 km at the equator) by obtaining parameters and inputs from the global
 306 hydrology and water resources model PCR-GLOBWB 2 (Sutanudjaja et al., 2018, See Table



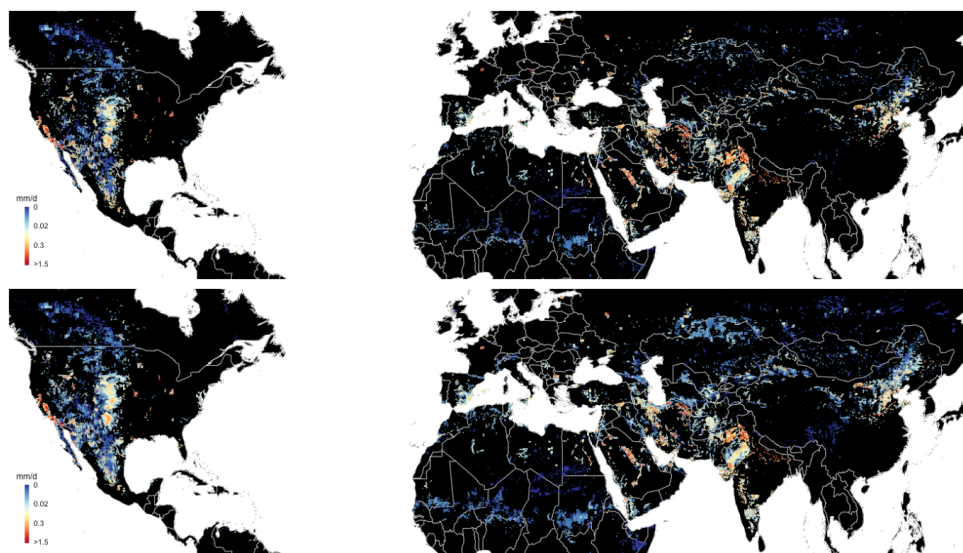
307 3). For the flux densities q , q_s , r , the discharge Q_i and the velocity v we used the average
 308 values over the period 2000-2015. The groundwater-surface water interaction parameter C is
 309 determined from the characteristic response time J of the groundwater reservoir in PCR-
 310 GLOBWB 2, which is based on the drainage theory of Kraijenhoff-van de Leur (1958). From
 311 this solution and Equation (2) it can be shown that $C=J/n$ (see Appendix B). Since the
 312 variables q_{crit} and t_{crit} depend heavily on the value of C we have also included the dataset of
 313 groundwater response time published by Cuthbert et al. (2019) to calculate the C value.
 314 Figure 4 shows the groundwater depletion rates $q-q_{crit}$ for the areas with non-sustainable
 315 groundwater withdrawal. The resulting patterns are remarkably similar to those calculated
 316 from previous global studies (Wada et al., 2012; Döll et al., 2014) and show the well-known
 317 hotspots of the world. Total depletion rates in Figure 4 are $158 \text{ km}^3 \text{ yr}^{-1}$ (top) and 166 km^3
 318 yr^{-1} (bottom), which are in the range of previous studies, e.g., $234 \text{ km}^3 \text{ yr}^{-1}$ (Wada et al.,
 319 2012; year 2000), $171 \text{ km}^3 \text{ yr}^{-1}$ (Sutanudjaja et al., 2018; 2000-2015) and $113 \text{ km}^3 \text{ yr}^{-1}$ (Döll
 320 et al., 2014; 2000-2009).

321

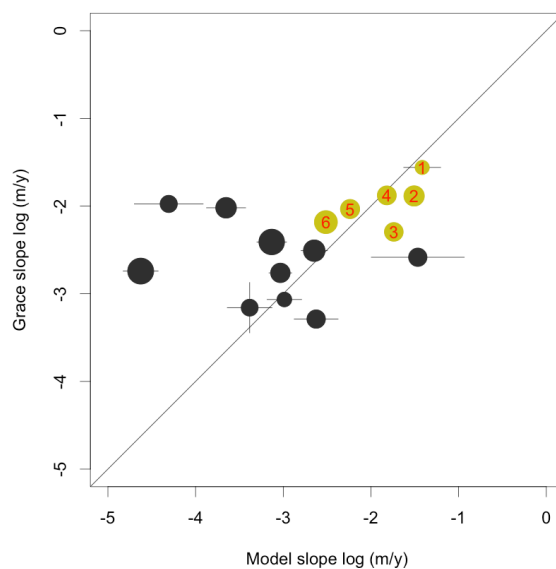
322 *Table 3. Parameter and input values used in global-scale analyses at 5 arc-minute cells. All*
 323 *inputs obtained from PCR-GLOBWB 2 (Sutanudjaja et al., 2018), except the C value*
 324 *obtained from PCR-GLOBWB and from Cuthbert et al. (2018).*

Parameter	Value
Surface water system	
A	Cell area 5 arc-minute cells (m^2)
q_s	Sum of surface runoff and interflow (m d^{-1}) of a cell
Q_i	Upstream discharge of a cell ($\text{m}^3 \text{ d}^{-1}$)
d	Stream depth (m) based on bankfull discharge
W	Stream width (m) based on bankfull discharge
v	Calculated from bankfull discharge and stream depth (m d^{-1}) assuming v to be dependent on terrain slope only.
Hydrogeology	
C	$C = J/n$ (days), with J the characteristic response time of the third reservoir (Sutanudjaja et al. 2018) or groundwater response times from Cuthbert et al. (2019).
n	Porosity values (-) from the groundwater reservoir in PCR- GLOBWB.
r	Net recharge (recharge minus capillary rise) (m d^{-1}).

325



326
327 *Figure 4. Average groundwater depletion rates ($q-q_{crit}$) over 2000-2015 at 5 arc-minute*
328 *resolution calculated with the data from Table 1. The top figure uses C-values from*
329 *Sutanudjaja et al. (2018) and the bottom figure of Cuthbert et al. (2019).*
330
331



332
333
334 *Figure 5. Comparison of depletion rates in Figure 4 (top) for major groundwater basins with*
335 *average depletion rates from GRACE. Size of the circles is proportional to aquifer area;*
336 *crosses are standard errors in estimated mean aquifer trends; 1: Central Valley (California);*
337 *2: Ganges-Brahmaputra basin; 3: Indus basin; 4: North China plane; 5. Ogallala (High*
338 *Plains) aquifer; 6. Arabian aquifer system.*

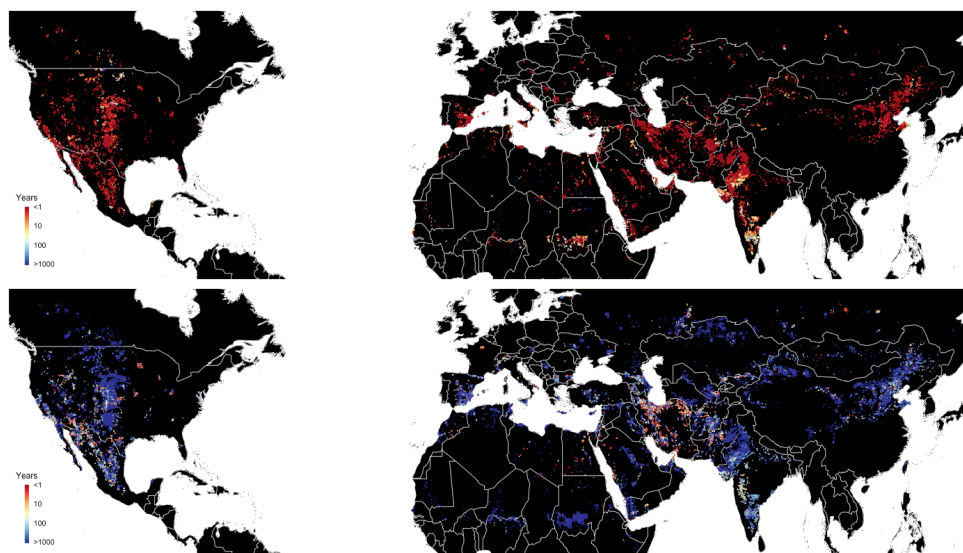


339 From the results in Figure 4 (top with C from PCR-GLOBWB 2) we computed average
340 depletion rates of the world's major aquifers subject to depletion (following Richey et al.,
341 2015) and compared these with average trends in total water storage (TWS) from GRACE
342 (Gravity Recovery and Climate Experiment) gravity anomalies over the period 2003-2015
343 (Figure 5). We used the JPL GRACE Mascon product RL05M (Wiese, 2015; Watkins et al.,
344 2015; Wiese et al., 2016). We did not correct TWS for changes in other hydrological stores,
345 assuming the latter to be approximately constant over a 13-year period in semi-arid areas
346 with limited surface water and TWS trends to mainly reflect groundwater depletion. Figure 5
347 shows that the estimated depletion rates are reasonably consistent with the GRACE estimates,
348 particularly for the known hotspot aquifers with the largest depletion. The aquifers whose
349 depletion rates are underestimated have estimated GRACE trends between 1-10 mm/year,
350 just above the accuracy limit of GRACE TWS trends (viz. Richey et al., 2015).

351

352 Figure 6 shows the time to critical transition t_{crit} from both datasets. It is quite striking that,
353 although the depletion rates are rather similar (Figure 4) between datasets, the critical
354 transition times are much larger for the Cuthbert et al. (2018) dataset, owing to its much
355 larger groundwater response times.

356

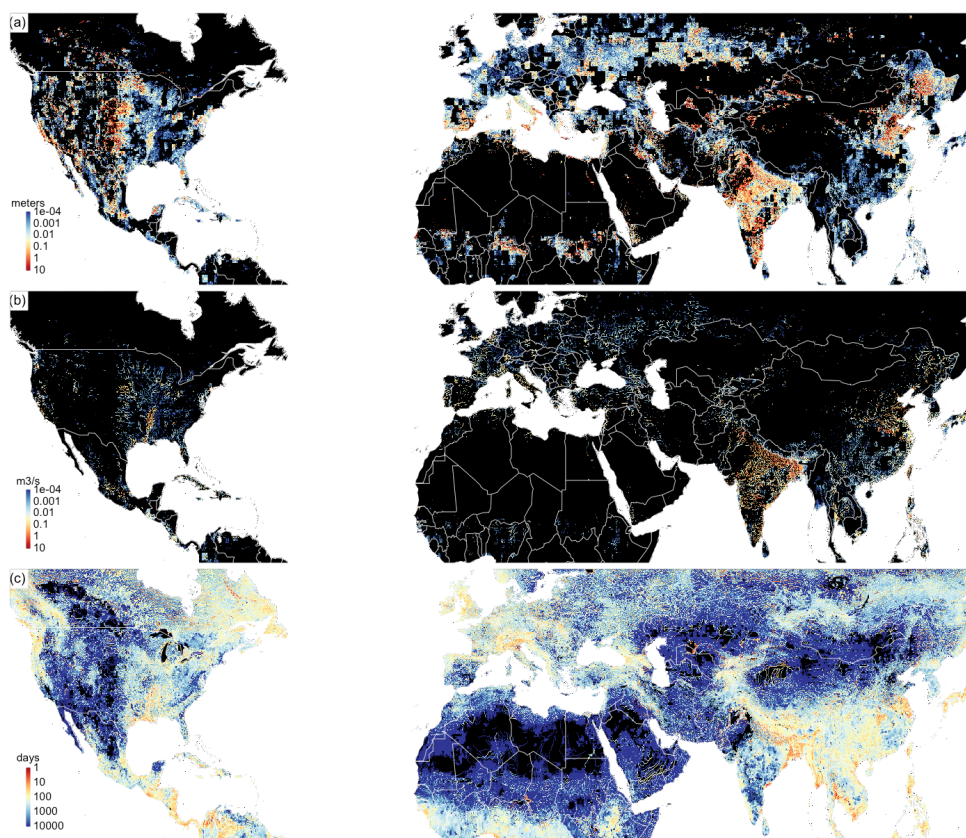


357

358 Figure 6. Critical transition times (Critical time at which the groundwater level becomes
359 disconnected from the stream after start of pumping, i.e. $h < h_s$ in case $q > q_{crit}$) calculated
360 with the data from Table 1. The top figure uses C -values from Sutanudjaja et al. (2018) and
361 the lower figure from Cuthbert et al. (2019).



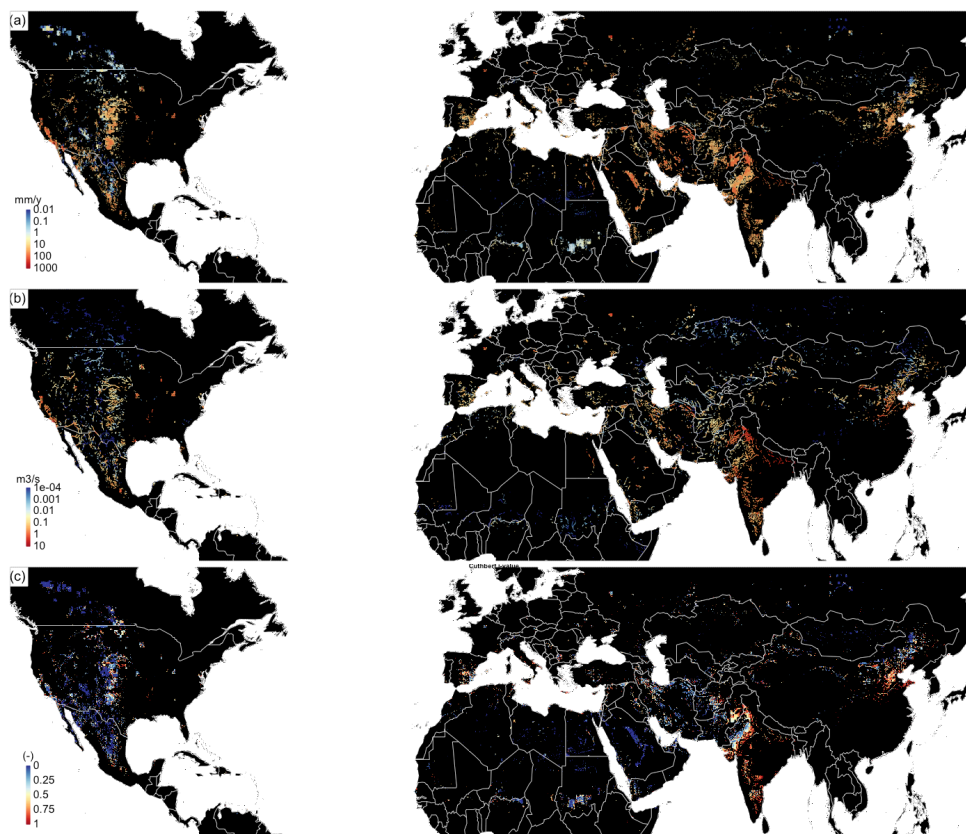
362 To further explore the global impacts of groundwater withdrawal we calculated relevant
363 output variables for the areas that have been identified as subject to sustainable groundwater
364 withdrawal ($q \leq q_{crit}$; Figure 7) and non-sustainable withdrawal ($q > q_{crit}$; Figure 8). Figure
365 7a shows the equilibrium water table decline from sustainable groundwater withdrawal. We
366 see the largest declines occurring in areas with larger groundwater withdrawals, which are
367 often close to the depletion areas (Figure 3) and coincide with regions with limited surface
368 water occurrence due to a semi-arid climate (higher C-values). In contrast, the equilibrium
369 decline in streamflow (Figure 7b) is focused in areas with significant groundwater
370 withdrawal and higher surface water densities (low C-values), which are those areas that have
371 a more semi-humid climate where both groundwater and surface water use are present. These
372 are also the areas with relatively short times to equilibrium (Figure 7c).



373
374 *Figure 7. Results for the areas with sustainable withdrawal rates ($q \leq q_{crit}$); (a) equilibrium*
375 *groundwater level decline (m); (b) equilibrium reduction of discharge ($\text{m}^3 \text{s}^{-1}$); (c) e-folding*
376 *time to complete capture (days); black areas are areas without groundwater withdrawal,*
377 *with non-sustainable groundwater withdrawal or negligible values.*



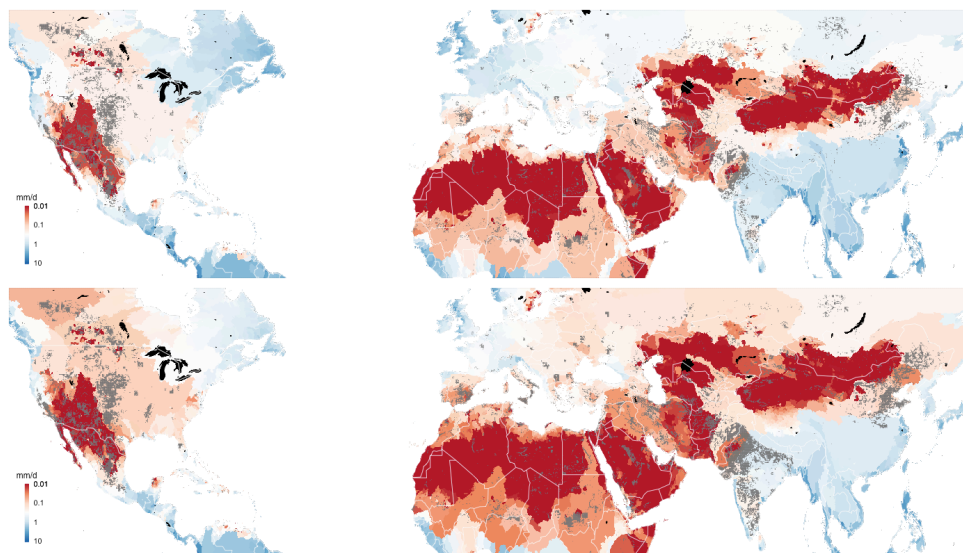
378 As expected, the groundwater decline rates under non-sustainable withdrawal (Figure 8a)
379 mirror the depletion rates (Figure 4). Estimates based on piezometers for major depleting
380 areas are in the order of 0.4-1.0 m yr⁻¹ in Southern California and the Southern High Plains
381 aquifer (Scanlon et al., 2012) and 0.1-1.0 m yr⁻¹ in the Gangetic plain (MacDonald et al.,
382 2016). Our estimates are in the lower end of those observed ranges, which could be partly
383 explained by the fact that, particularly in the U.S., groundwater withdrawal is from semi-
384 confined aquifers, leading to a larger head decline per volume out of storage than follows
385 from the specific yields used in our conceptual model. The largest change in streamflow and
386 the highest fraction of capture are found in areas where groundwater depletion coincides with
387 the presence of surface water, e.g. such as the Northern and Eastern part of the Ogallala
388 aquifer, the Indus basin and southern India.
389



390
391 *Figure 8. Results for the areas with non-sustainable withdrawal rates ($q > q_{crit}$); (a)*
392 *groundwater level decline rate (mm yr⁻¹); (b) equilibrium reduction of discharge (m³ s⁻¹); (c)*
393 *fraction of capture (-); black areas are areas without groundwater withdrawal, with*
394 *sustainable groundwater withdrawal or with negligible values.*



395 As the proverbial *pièce de résistance*, Figure 9 (top) summarizes the sustainable limits to
 396 groundwater withdrawal for the major river basins of the world. In Figure 9a the median
 397 value of q_{crit} is plotted for the major basins in the world (sub-watershed level of HydroBasins,
 398 Lehner et al., 2008) together with the areas where groundwater withdrawal is on average non-
 399 sustainable over the years 2000-2015. This figure provides, at first order, a global map of the
 400 maximum limit to physically sustainable groundwater withdrawal rates. The parts of the
 401 world where the critical withdrawal rates are very small largely coincide with the band of
 402 countries that experience high values of water stress (Hofsté et al., 2019). This shows that
 403 there is little room in these areas to supplement water demand with sustainable use of
 404 groundwater.



405
 406 *Figure 9. Global limits to sustainable groundwater withdrawal rate; top: limit to physically*
 407 *sustainable groundwater withdrawal mapped as the median q_{crit} per sub-basin (based on*
 408 *Hydro-basins: Lehner et al., 2008), grey-shaded areas are those for which $q > q_{crit}$; bottom:*
 409 *limit to ecologically sustainable groundwater withdrawal mapped as the median q_{eco} per sub-*
 410 *basin, grey-shaded areas are those $q > q_{eco}$.*

411
 412 The ecological limits to groundwater withdrawal, q_{eco} , can be defined as the withdrawal rate
 413 that is low enough to prevent streamflow from dropping below some environmental flow
 414 limit Q_{env} , i.e. a value that is high enough to safeguard the integrity of the aquatic ecosystems
 415 (Linnansaari et al. 2013; Pastor et al 2014). The value of q_{eco} can be calculated by inverting
 416 Equation (A14) and taking $Q(\infty) < Q_{env}$:

417

$$q_{eco} = \frac{(Q_i + (q_s + r)A) - Q_{env}}{A} \quad (4)$$



418 We note that environmental flows are usually defined during low flow conditions (Pastor et
419 al 2014; Gleeson and Richter, 2018), so it may be more appropriate to use the value of $Q(\infty)$
420 as the average over the summer half year instead of yearly averages. If we assume that the
421 average streamflow regime follows a cosine function with a period of 1 year, then the
422 average (natural) streamflow Q_s in summer would be equal to:

$$423 \quad Q_s = \left(1 - \frac{2}{\pi}\right) [(Q_i + (q_s + r)A)] \quad (5)$$

424 and q_{eco} becomes:

$$425 \quad q_{eco} = \frac{\left(1 - \frac{2}{\pi}\right) [Q_i + (q_s + r)A] - Q_{env}}{A} \quad (5)$$

426 In Figure 9 (bottom) we have used plotted q_{eco} using, as an example, Q_{env} to be 20% of the
427 average natural summer streamflow Q_s . The resulting map can be seen as a first order
428 approximation of the limits to ecologically sustainable groundwater withdrawal. In most
429 cases, $q_{eco} < q_{crit}$ as is also evident from the larger grey-shaded areas in the bottom figure
430 compared to the top figure. The results suggest that supplementing water demand by
431 groundwater use in the world's water stressed areas is limited under ecological constraints.

432

433 **4. Discussion and conclusions**

434

435 We have introduced a conceptual analytical framework that describes to what extent
436 groundwater withdrawal affects groundwater heads and streamflow under changing regimes
437 of groundwater-surface water interaction. It is likely the simplest analytical form that can be
438 devised to describe the effects of groundwater pumping at the larger scale. It cuts down a
439 many-faceted and complex problem to its bare essentials and reduces it to lumped, piece-wise
440 linear problem with time-invariant forcing. Yet, despite this simplicity, the framework is able
441 to provide a rich tableau of hydrologically, economically and ecologically relevant outputs,
442 produces results at the global scale that are remarkably similar to those obtained with global
443 hydrological models, with the advantage of a significant reduction in data and computational
444 requirements. In addition, the estimated groundwater depletion rates compare reasonably
445 well with estimates from an independent satellite-based source like GRACE and average in-
446 situ measurements for some major aquifer systems. As such, the framework can be used in
447 e.g. GIS-based scoping studies to provide first-order estimates of the regional-scale impact of
448 future groundwater pumping on groundwater levels, or to set regional-scale ecological or
449 physical limits to groundwater pumping. Another possible application is in hydroeconomic
450 modelling, where the equations in Table 1 can be used as regionally varying hydrological



451 response functions (Harou et al., 2009; MacEwan et al., 2017) in hydroeconomic
452 optimization – where model evaluations need to be fast - in order to infer socially optimal
453 pumping rates that include environmental externalities.
454

455 Clearly, many complicating factors are neglected in our approach, e.g.: underground spatial
456 heterogeneity, including the occurrence of multiple aquifer systems and semi-confined layers
457 that occur in many important alluvial groundwater basins; the variable depth and topology of
458 the surface water system and the intermittent nature of many streams in semi-arid to semi-
459 humid areas; and the locations of the wells with respect to the streams. Of these, the neglect
460 of confining layers may be one of the more crucial limitations of the approach. For instance,
461 a considerable part of the groundwater used for irrigation in the big alluvial basins of the U.S.
462 (e.g. Ogallala and Central Valley of California), where farmers have the financial resources
463 to drill deep wells (Perrone and Jasechko, 2019), is pumped from deeper confined aquifers.
464 This means that the groundwater-surface water interaction is limited to the large rivers and
465 lakes only and that head decline per volume water pumped is larger than in phreatic
466 conditions. It would in principle be possible to include the effect of a confining layer by using
467 a larger value of the groundwater-surface water resistance parameter C , a smaller value of
468 recharge r and a storage coefficient instead of specific yield. Similarly, the impacts of
469 seasonably variable boundary conditions of q , q_s and Q_i could be taken into account by simple
470 convolution, considering that the groundwater level responses $h(t)$ and dh/dt (Table 1) are
471 respectively step and impulse responses of a linear system. Also, the effects of multiple
472 streams with variable stream bottom elevations could be included by extending the piecewise
473 linearization of Equation (2) to more domains (e.g. Bierkens and te Stroet, 2007). However,
474 we argue that such extensions are not in the spirit of the conceptual framework developed,
475 which intends to provide first order sensitivities at larger scales. If the addition of complexity
476 is needed to provide more accurate assessments for a specific case, it would be more logical
477 to build a tailor-made numerical groundwater flow model.
478

479 The similarity of the groundwater depletion estimates by our conceptual analytical
480 framework with estimates obtained by global hydrological models is not as surprising as it
481 seems. In fact, the way the groundwater-surface water system is modelled in Figure 1 is quite
482 similar to how the groundwater reservoirs and their interaction with surface water have been
483 implemented in global hydrological models such as PCR-GLOBWB (De Graaf et al., 2015)
484 and WGHM (Döll et al., 2014) (see also Appendix B). Since the groundwater dynamics of all



485 models are (piece-wise) linear and groundwater recharge in our model is applied directly in
486 Equation (1) – i.e. the non-linear responses of the soil system to precipitation and evaporation
487 is bypassed -, forcing our model with average fluxes r , q , Q_i and q_s and using the parameter J
488 from PCR-GLOBWB yields almost the same depletion rates as from the time varying model
489 simulations with PCR-GLOBWB. The small difference between our estimate ($158 \text{ km}^3 \text{ yr}^{-1}$)
490 and the value from PCR-GLOBWB 2 (Sutanudjaja et al., 2018) ($171 \text{ km}^3 \text{ yr}^{-1}$) is explained
491 by a resulting non-linearity not accounted for: during dry periods some of the streams in the
492 PCR-GLOBWB run dry and do not contribute to the concentrated recharge flux.

493

494 We end with pressing that a global application of our conceptual analytical framework is not
495 restricted to the use of data from the PCR-GLOBWB repository. The necessary fluxes r , q ,
496 Q_i and q_s can also be obtained from other repositories of multi-model re-analyses such as
497 Earth2Observe (Schellekens et al., 2017) and from the combination of remotely sensed
498 estimates of hydrological variables (Lettenmaier et al., 2015; McCabe et al., 2017), e.g.
499 estimating recharge and surface runoff from remotely sensed precipitation, evaporation and
500 soil moisture change, and using high-resolution global datasets on discharge (Barbarossa et
501 al., 2018) and river bed dimensions (Allen and Pavelsky, 2018; Lehner et al., 2018).

502

503



504 **Data availability.**

505 The data used in the global assessments provided by PCR-GLOBWB 2 can downloaded
506 from: <https://doi.org/10.4121/uuid:e3ead32c-0c7d-4762-a781-744dbdd9a94b>. The
507 groundwater response times of Cuthbert et al. (2019) can be found on:
508 <https://doi.org/10.6084/m9.figshare.7393304> GRACE data used for validation are obtained
509 from: <https://doi.org/10.5067/TEMSC-OCL05>

510

511 **Author contributions.**

512 MB conceived and designed the study. NW and MB performed the calculations. EHS
513 performed the model validation. MB wrote the paper. All authors read, commented on, and
514 revised the manuscript.

515

516 **Competing interests.**

517 The authors declare that they have no conflict of interest.

518

519 **Acknowledgements.**

520 Niko Wanders acknowledges funding from NWO 016.Veni.181.049.

521



522 **References**

- 523
- 524 Allen, H. and Pavelsky, M. (2018). Global extent of rivers and streams. *Science* 361, 585-
- 525 588.
- 526 Alley, W.M., Reilly, T. E. and Franke, O. L. (1999). Sustainability of groundwater resources
- 527 *United States Geological Survey Circular* 1186.
- 528 Barbarossa, V., Huijbregts, M., Beusen, A. *et al.* (2018). FLO1K, global maps of mean,
- 529 maximum and minimum annual streamflow at 1 km resolution from 1960 through
- 530 2015. *Sci Data* 5, 180052.
- 531 Bierkens, M.F.P. and Te Stroet, C.B.M (2007). Modelling non-linear water table dynamics
- 532 and specific discharge through landscape analysis. *J. Hydrol.* 332, 412– 426.
- 533 Bierkens, M.F.P. and Wada, Y. (2019). Non-renewable groundwater use and groundwater
- 534 depletion: a review. *Environ. Res. Lett.* 14 063002.
- 535 Cuthbert, M.O., Gleeson, T., Moosdorf, N. *et al.* (2019). Global patterns and dynamics of
- 536 climate–groundwater interactions. *Nature Clim. Change* 9, 137–141.
- 537 de Graaf, I.E.M., van Beek, L.P.H., Wada, Y., and Bierkens, M.F.P. (2014). Dynamic
- 538 attribution of global water demand to surface water and groundwater resources: Effects of
- 539 abstractions and return flows on river discharges, *Adv. Water Resour.* 64, 21–33.
- 540 de Graaf, I.E.M., Gleeson, T., van Beek, L.P.H., Sutanudjaja, E.H. and Bierkens, M.F.P.
- 541 (2019). Environmental flow limits to global groundwater pumping. *Nature* 574, 90-108.
- 542 Döll, P., Müller Schmied, H., Schuh, C., Portmann, F.T. and Eicker, A. (2014), Global-scale
- 543 assessment of groundwater depletion and related groundwater abstractions: Combining
- 544 hydrological modeling with information from well observations and GRACE satellites.
- 545 *Water Resour. Res.* 50, 5698–5720.
- 546 Elmore, A.J., Manning, S.J., Mustar, J.F. and Craine J.M. (2006). Decline in alkali meadow
- 547 vegetation cover in California: the effect of groundwater extraction and drought. *J. Appl.*
- 548 *Ecol.* 43, 770–9.
- 549 Gleeson, T., Moosdorf, N., Hartmann, J., and van Beek, L. P. H. (2014). A glimpse beneath
- 550 earth's surface: GLObal HYdrogeology MaPS (GLHYMPS) of permeability and porosity,
- 551 *Geophys. Res. Lett.*, 41, 3891–3898
- 552 Gleeson, T. and Richter, B. (2018). How much groundwater can we pump and protect
- 553 environmental flows through time? Presumptive standards for conjunctive management of
- 554 aquifers and rivers. *River Res. Appl.* 34 83–92.
- 555 Godfray, H.C.J., Beddington, J.R, Crute, I.R., Haddad, L., Lawrence, D., Muir, J.F. *et al.*
- 556 (2010). Food security: The challenge of feeding 9 billion people. *Science* 327, 812–818.
- 557 Harou, J.J., Pulido-Velazquez, M., Rosenberg, D.E., Medellín-Azuara, J., Lund, J. R. and
- 558 Howitt, R. E. (2009). Hydro-economic models: concepts, design, applications, and future
- 559 prospects. *J. Hydrol.* 375 627–43.
- 560 Hofste, R.W.,Kuzma, S., Walker, S., Sutanudjaja, E.H., Bierkens, M.F.P., Kujiper, M.J.M.,
- 561 Sanchez, M.F., van Beek, R., Wada, Y., Rodríguez, S.G. (2019). *Aqueduct 3.0: Updated*
- 562 *Decision-Relevant Global Water Risk Indicators*; Technical Note World Resources
- 563 Institute, Washington, DC, USA, 2019; <https://www.wri.org/publication/aqueduct-30>
- 564



- 565 Huang, S.-H., Yang, T. and Yeh, H.-D. (2018). Review of analytical models to stream
566 depletion induced by pumping: Guide to model selection. *J. Hydrol* 561, 277-285.
- 567 Hunt, B., 2003. Unsteady stream depletion when pumping from semiconfined aquifer. *J.*
568 *Hydrol. Eng.-ASCE* 8, 12–19
- 569 Konikow, L.F. and Leake, S.A. (2014). Depletion and capture: Revisiting “the source of
570 water derived from wells”. *Groundwater* 52, 100–111.
- 571 Kraijenhoff van de Leur, D. A. (1958). A study of non-steady ground-water flow with special
572 reference to the reservoir-coefficient, *De Ingenieur* 19, 87–94.
- 573 Lehner, B., Verdin, K. and Jarvis, A. (2008). New global hydrography derived from
574 spaceborne elevation data. *Eos* 89, 93–94.
- 575 Lehner, B., Ouellet Dallaire, C., Ariwi, J., Grill, G., Anand, M., Beames, P., Burchard-
576 Levine, V., Maxwell, S., Moidu, H., Tan, F. and Thieme, M. (2019). Global hydro-
577 environmental sub-basin and river reach characteristics at high spatial resolution. *Sci.*
578 *Data* 6, 283.
- 579 Lettenmaier, D. P., Alsdorf, D., Dozier, J., Huffman, G.J., Pan, M. and Wood, E.F. (2015).
580 Inroads of remote sensing into hydrologic science during the WRR era. *Water Resour.*
581 *Res.* 51, 7309–7342.
- 582 Linnansaari T, Monk, W.A., Baird, D.J. and Curry R. A. (2013). *Review of Approaches and*
583 *Methods to Assess Environmental Flows Across Canada and Internationally*. Canadian
584 Science Advisory Secretariat, Research Document 2012/039 (New Brunswick:
585 Department of Fisheries and Oceans Canada)
- 586 MacDonald, A., Bonsor, H., Ahmed, K. *et al.* (2016). Groundwater quality and depletion in
587 the Indo-Gangetic Basin mapped from *in situ* observations. *Nature Geosci.* 9, 762–766.
- 588 MacEwan, D., Cayar, M., Taghavi, A., Mitchell, D., Hatchett, S. and Howitt, R. (2017).
589 Hydroeconomic modeling of sustainable groundwater management. *Water Resour. Res.* 53
590 2384–403
- 591 McCabe, M. F., Rodell, M., Alsdorf, D. E., Miralles, D. G., Uijlenhoet, R., Wagner, W.,
592 Lucieer, A., Houborg, R., Verhoest, N. E. C., Franz, T. E., Shi, J., Gao, H., and Wood, E.
593 F. (2017). The future of Earth observation in hydrology. *Hydrol. Earth Syst. Sci.* 21,
594 3879–3914.
- 595 Mukherjee, A., Bhanja, S.N. and Wada, Y. (2018). Groundwater depletion causing reduction
596 of baseflow triggering Ganges river summer drying. *Sci. Rep.* 8, 12049.
- 597 Pastor, A.V., Ludwig, F., Biemans, H., Hoff, H. and Kabat, P. (2014). Accounting for
598 environmental flow requirements in global water assessments. *Hydrol. Earth Syst. Sci.* 18
599 5041–59.
- 600 Perrone, D. and Jasechko, S. (2019). Deeper well drilling an unsustainable stopgap to
601 groundwater depletion. *Nat. Sustain.* 2, 773–782.
- 602 Richey, A. S., Thomas, B. F., Lo, M.-H., Reager, J.T., Famiglietti, J.S., Voss, K., Swenson,
603 S. and Rodell, M. (2015). Quantifying renewable groundwater stress with GRACE. *Water*
604 *Resour. Res.* 51, 5217–5238.
- 605 Runhaar ,H., Witte, J.P.M. and Verburg, P. (1997). Groundwater level, moisture supply, and
606 vegetation in the Netherlands. *Wetlands* 17, 528–38.



- 607 Scanlon, B.R., Faunt, C.C., Longuevergne, L., Reedy, R.C., Alley, W.M., McGuire, V.L. and
608 McMahon, P.B. (2012). Groundwater depletion and sustainability of irrigation in the U.S.
609 High Plains and Central Valley. *P. Natl. Acad. Sci. U.S.A.* 109, 9320–9325.
- 610 Schellekens, J., Dutra, E., Martínez-de la Torre, A., Balsamo, G., van Dijk, A., Sperna
611 Weiland, F., Minvielle, M., Calvet, J.-C., Decharme, B., Eisner, S., Fink, G., Flörke, M.,
612 Peßenteiner, S., van Beek, R., Polcher, J., Beck, H., Orth, R., Calton, B., Burke, S.,
613 Dorigo, W., and Weedon, G. P. (2017). A global water resources ensemble of hydrological
614 models: the earth2Observe Tier-1 dataset. *Earth Syst. Sci. Data* 9, 389–413.
- 615 Shafroth P.B., Stromberg J.C. and Patten D.T. (2000). Woody riparian vegetation response to
616 different alluvial water table regimes Western North. *Am. Nat.* 60, 66–76.
- 617 Siebert, S., Kummu, M., Porkka, M., Döll, P., Ramankutty, N. and Scanlon, B.R. (2015). A
618 global data set of the extent of irrigated land from 1900 to 2005. *Hydrol. Earth Syst. Sci.*
619 19, 1521–1545.
- 620 Sutanudjaja, E. H., van Beek, R., Wanders, N., Wada, Y., Bosmans, J. H. C., Drost, N., van
621 der Ent, R. J., de Graaf, I. E. M., Hoch, J. M., de Jong, K., Karssenbergh, D., López López,
622 P., Peßenteiner, S., Schmitz, O., Straatsma, M. W., Vannamettee, E., Wisser, D., and
623 Bierkens, M. F. P. (2018). PCR-GLOBWB 2: a 5 arcmin global hydrological and water
624 resources model. *Geosci. Model Dev.* 11, 2429–2453.
- 625 Theis, C.V. (1940). The source of water derived from wells. *Civ. Eng.* 10, 277–280.
- 626 Bredehoeft, J.D. (2002). The water budget myth revisited: why hydrogeologists model.
627 *Groundwater* 40, 340–345.
- 628 Wada, Y., van Beek, L.P.H. van Kempen, C.M., Reckman, J.W.T., Vasak, S., and Bierkens,
629 M.F.P. (2010). Global depletion of groundwater resources. *Geoph. Res. Lett.* 37, L20402.
- 630 Wada, Y., van Beek, L.P.H. and Bierkens, M. F. P (2012). Nonsustainable groundwater
631 sustaining irrigation: A global assessment, *Water Resour. Res.*, 48, W00L06,
- 632 Wada Y., van Beek, L.P.H., Wanders and Bierkens M.F.P. (2013). Human water
633 consumption intensifies hydrological drought worldwide. *Environ. Res. Lett.* 8, 034036.
- 634 Wada Y. (2016). Modeling Groundwater Depletion at Regional and Global Scales: Present
635 State and Future Prospects. *Surv. Geophys.* 37, 419–451.
- 636 Watkins, M.M., Wiese, D.N., Yuan, D.-N., Boening, C., and Landerer, F.W. (2015).
637 Improved methods for observing Earth's time variable mass distribution with GRACE
638 using spherical cap mascons. *J. Geophys. Res.-Solid* 120, 2648–2671.
- 639 Wiese, D.N. (2015). GRACE monthly global water mass grids NETCDF RELEASE 5.0,
640 Version 5.0, PO.DAAC, CA, USA, Dataset, available at:[https://doi.org/10.5067/TEMSC-](https://doi.org/10.5067/TEMSC-OCL05)
641 [OCL05](https://doi.org/10.5067/TEMSC-OCL05) (last access: 15 September 2017).
- 642 Wiese, D.N., Landerer, F.W., and Watkins, M.M. (2016). Quantifying and reducing leakage
643 errors in the JPL RL05M GRACE mascon solution. *Water Resour. Res.* 52, 7490–7502.
- 644 Winter, T.C., Harvey, J.W., Franke, O.L. and Alley, W.A. (1998). *Ground water and surface*
645 *water: A single resource*. U.S. Geol. Surv. Circ., 1139.
- 646 Yin, L., Zhou, Y., Xu, D., Zhang, J., Wang, X., Ma, H. and Dong, J. (2018). Response of
647 phreatophytes to short-term groundwater withdrawal in a semiarid region: Field
648 experiments and numerical simulations *Ecohydrol.* 11, e1948.



- 649 Zipper, S.C., Dallemagne, T., Gleeson, T., Boerman, T.C., and Hartmann, A. (2018).
650 Groundwater pumping impacts on real stream networks: Testing the performance of
651 simple management tools. *Water Resour. Res.* 54, 5471-5486.



652 **Appendix A: Conceptual model for regional-scale groundwater pumping**
653 **with groundwater-surface water interaction**

654
655

656 **A1. Basic equations**

657 We repeat the three basic equations that make up the conceptual model regional-scale
658 groundwater pumping with groundwater-surface water interaction:

659 The groundwater head as described with the total aquifer mass balance:

660
$$n \frac{dh}{dt} = r + F_{gw \leftrightarrow sw}(h) - q \quad (A1)$$

661 The groundwater - surface water flux:

662
$$F_{gw \leftrightarrow sw}(h) = \begin{cases} -\frac{h-h_s}{c} & h \geq d \\ \frac{h_s-d}{c} & h < d \end{cases} \quad (A2)$$

663 The surface water balance:

664
$$Q = Wv(h_s - d) = Q_i + q_s A + F_{gw \leftrightarrow sw}(h)A \quad (A3)$$

665

666 **A2. The case $h(t) \geq d$ and $q < q_{crit}$**

667 We will start by analyzing the case that $h \geq d$, i.e. the groundwater level is attached to the
668 surface water body. We further assume that $q < q_{crit}$, i.e. the groundwater withdrawal is such
669 that the groundwater level never falls below the surface water bottom level d . In this case, the
670 surface water flux Q (m³/day) is related to the groundwater and surface water level as follows
671 (See Figure A1):

672
$$Q = Wv(h_s - d) = Q_i + q_s A + \frac{h-h_s}{c} A \quad (A3)$$

673 with

674 A : The area over (sub-)aquifer considered (m²)

675 q_s : surface runoff (m d⁻¹)

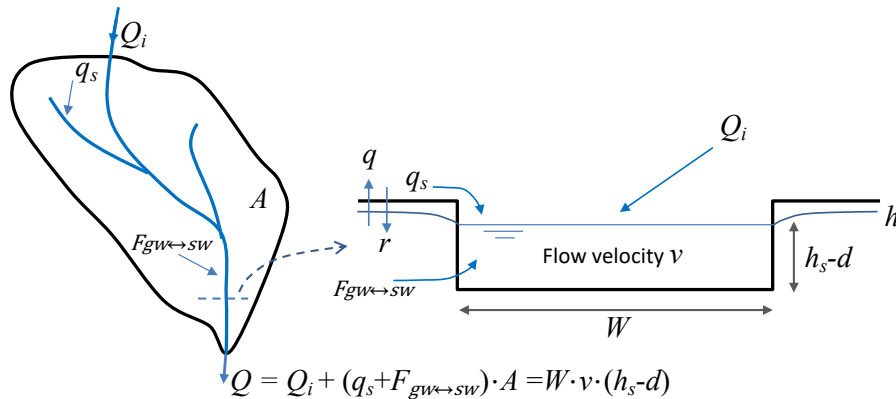
676 Q_i : influx of surface water from upstream (m³ d⁻¹)

677 W : Stream width (m)

678 d : Bottom elevation stream (m)

679 v : Stream flow velocity (m d⁻¹)

680



681

682 *Figure A1. Contributing fluxes to streamflow.*

683

684 Collecting h_s on one side and the other terms on right side results in the following relation
 685 between surface water height and groundwater head:

$$686 \quad h_s(t) = \alpha + \beta h(t) \quad (A4)$$

687 with

$$688 \quad \alpha = \frac{Q_i C + q_s A C + W v d C}{W v C + A} \quad (A5)$$

$$689 \quad \beta = \frac{A}{W v C + A} \quad (A6)$$

690 From (A1) and (A2) the differential equation for groundwater level gives:

$$691 \quad n \frac{dh}{dt} = r - \frac{h - h_s}{c} - q \quad (A7)$$

692 And after substituting (A4)

$$693 \quad \Rightarrow n \frac{dh}{dt} = \left(r + \frac{\alpha}{c} - q \right) - \left(\frac{1 - \beta}{c} \right) h \quad (A8)$$

694 From (A8) follows the steady-state groundwater level under natural conditions ($q = 0$ and
 695 $dh/dt = 0$):

$$696 \quad \bar{h}_{nat} = \frac{rC + \alpha}{1 - \beta} \quad (A9)$$

697 Solving differential equation (A8) for initial condition (A9) then yields:

$$698 \quad h(t) = \frac{rC + \alpha}{1 - \beta} - \left(\frac{qC}{1 - \beta} \right) \left[1 - e^{-\left(\frac{1 - \beta}{nC} \right) t} \right] \quad (A10)$$

699 Which also gives the equilibrium groundwater level for $t \rightarrow \infty$:

$$700 \quad h(\infty) = \frac{rC + \alpha - qC}{1 - \beta} \quad (A11)$$

701 The surface water level with time is given by (A4) and the final equilibrium surface water
 702 follows from (A4) and (A11) as:



$$703 \quad h_s(\infty) = \alpha + \frac{\beta(rc + \alpha - qC)}{1 - \beta} \quad (A12)$$

704 The surface water discharge as a function of time follows from combining (A3) and (A4):

$$705 \quad Q(t) = Q_i + q_s A - \frac{A\alpha}{c} + \frac{A(1-\beta)}{c} h(t) \quad (A13)$$

706 with $h(t)$ given by (A10). The equilibrium discharge is obtained by substituting (A11) for

707 $h(\infty)$ in (A13):

$$708 \quad Q(\infty) = Q_i + (q_s + r - q)A \quad (A14)$$

709 Which also follows logically from the water balance.

710

711 **A3. The critical withdrawal rate q_{crit}**

712 The critical withdrawal rate determines whether at larger times the water table drops below

713 the bottom of the surface and moves to the physically non-sustainable regime. We seek q

714 such that $h(\infty) = d$:

$$715 \quad \frac{rc + \alpha - qC}{1 - \beta} = d \quad (A15)$$

716 From which follows:

$$717 \quad q = \frac{rc + \alpha - d(1 - \beta)}{C} \quad (A16)$$

718 Substituting α and β yields after some manipulation:

$$719 \quad q_{\text{crit}} = r + \frac{Q_i + q_s A}{WvC + A} \quad (A17)$$

720

721 **A4. Critical transition time t_{crit} in case $q > q_{\text{crit}}$**

722 In case $q > q_{\text{crit}}$ at some time after pumping (t_{crit}) the groundwater level will fall below the

723 bottom elevation d of the surface water. Before that time, it follows the water table decline

724 according to (A10). So, we can find t_{crit} by solving it from:

$$725 \quad h(t_{\text{crit}}) = \frac{rc + \alpha}{1 - \beta} - \left(\frac{qC}{1 - \beta} \right) \left[1 - e^{-\left(\frac{1 - \beta}{nC} \right) t_{\text{crit}}} \right] = d \quad (A18)$$

726 Solving an equation of the form $a - b[1 - e^{-cx}] = d$ gives as solution: $x = \frac{1}{c} \ln \left(\frac{b}{d - a + b} \right)$

727 from which follows from (A18):

$$728 \quad t_{\text{crit}} = \frac{nC}{1 - \beta} \ln \left(\frac{qC}{qC - (rc + \alpha) + d(1 - \beta)} \right) \quad (A19)$$

729

730 **A5. The case $q > q_{\text{crit}}$ and $t > t_{\text{crit}}$ ($h(t) < d$)**

731 In case the water table is below the bottom elevation of the stream, the water balance of the

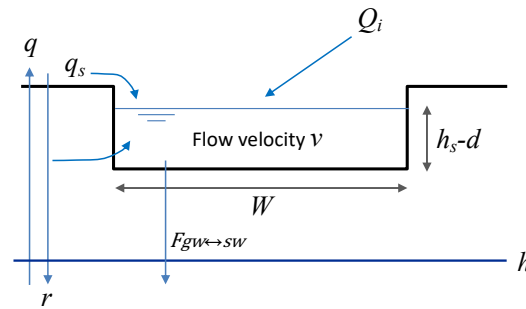
732 stream reads (see Fig. A2):



$$733 \quad Q = Wv(h_s - d) = Q_i + q_s A - \frac{h_s - d}{c} A \quad (A20)$$

734 From which we can derive an equation for the minimum and constant elevation of the surface
 735 water level (valid for $t > t_{crit}$):

$$736 \quad h_s = d + \frac{(Q_i + q_s A)C}{WvC + A} \quad (A21)$$



737

738 *Figure A2. Water balance of a stream in case $q > q_{crit}$ and $t > t_{crit}$ ($h(t) < d$)*

739

740 The differential equation describing the change in groundwater with time now becomes:

$$741 \quad n \frac{dh}{dt} = r - q + \frac{h_s - d}{c} \quad (A22)$$

742 Substituting $h_s - d$ from (A21) then yields an equation for the groundwater decline rate:

$$743 \quad \frac{dh}{dt} = \frac{r - q}{n} + \frac{(Q_i + q_s A)}{n(WvC + A)} \quad (A23)$$

744 which is always negative since $q > q_{crit}$. With initial condition $h(t_{crit}) = d$ one obtains from
 745 (A23) and equation for $h(t)$, $t > t_{crit}$:

$$746 \quad h(t) = d + \left[\frac{r - q}{n} + \frac{(Q_i + q_s A)}{n(WvC + A)} \right] (t - t_{crit}) \quad (A24)$$

747

748 **A5. Sources of pumped groundwater: $q < q_{crit}$ or $t < t_{crit}$ ($h(t) \geq d$)**

749 When neglecting direct evaporation from groundwater, the sources of pumped groundwater
 750 in case $q < q_{crit}$ either come out of storage or from recharge that does not contribute to
 751 streamflow. The latter is called “capture”. From the water balance (A1) we thus find:

$$752 \quad q = r + F_{gw \leftrightarrow sw}(h(t)) - n \frac{dh}{dt} \quad (A25)$$

753 The first two terms constitute the water pumped from capture (with $F_{gw \leftrightarrow sw}$ negative in case
 754 $h > h_s$ and positive when $h < h_s$) and the second term the water out of storage. Furthermore,
 755 from differentiation of (A10) we have:



$$756 \quad n \frac{dh}{dt} = -qe^{-\left(\frac{1-\beta}{nC}\right)t} \quad (A26)$$

757 Combining (A26) and (A25) then gives (since capture + out of storage add up to q):

758

$$759 \quad q = \underbrace{q \left(1 - e^{-\left(\frac{1-\beta}{nC}\right)t}\right)}_{r + F_{gw \leftrightarrow sw}} + \underbrace{qe^{-\left(\frac{1-\beta}{nC}\right)t}}_{-n \frac{dh}{dt}} \quad (A27)$$

760

761

762 This shows that the fraction groundwater taken out of storage reduces over time until head
 763 decline stops and all water comes out of capture.

764

765 **A6. Sources of pumped groundwater: $q > q_{crit}$ and $t > t_{crit}$ ($h(t) < d$)**

766 In case $q > q_{crit}$ and $t < t_{crit}$ the sources of pumped groundwater follow (A27). After the
 767 groundwater table falls below the bottom elevation of the stream and $t > t_{crit}$ the sources of
 768 water follow from (A23):

$$769 \quad n \frac{dh}{dt} = r - q + \frac{(Q_i + q_s A)}{(WvC + A)} \quad (A28)$$

770 And therefore:

$$771 \quad q = r + \frac{(Q_i + q_s A)}{(WvC + A)} - n \frac{dh}{dt} \quad (A29)$$

772 Since the third term is the storage change and capture plus storage change add up to q we
 773 have:

$$774 \quad q = \underbrace{r + \frac{(Q_i + q_s A)}{(WvC + A)}}_{r + F_{gw \leftrightarrow sw}} + \underbrace{q - \left(r + \frac{(Q_i + q_s A)}{(WvC + A)}\right)}_{-n \frac{dh}{dt}} \quad (A30)$$

775

776

777 which shows that at after $t > t_{crit}$ the ratio of pumping from capture (i.e. recharge and surface
 778 water leakage) and storage change becomes constant.

779

780



781 **Appendix B: Relationship between groundwater response time J and**
782 **drainage resistance C**

783
784 In PCR-GLOBWB 2 (Sutanudjaja et al., 2018) and in similar global hydrological models, the
785 relationship between groundwater discharge Q_g ($\text{m}^3 \text{m}^{-2} \text{d}^{-1}$) and the volume V_g (m^3/m^2)
786 stored in the groundwater store is given by a simple linear relationship:

$$787 \quad Q_g = \frac{V_g}{J} \quad (\text{B1})$$

788
789 With J the characteristic response time of the groundwater system (e-folding time of the
790 recession) (days). In some of the global models J is obtained by calibration to low flows or
791 recession curves. In PCR-GLOBWB it is calculated from transient drainage theory of
792 Kraijenhoff-van de Leur (1958) as:

$$793 \quad J = \frac{nL^2}{\pi^2 T} \quad (\text{B2})$$

794
795 with n the drainable porosity or specific yield, L the average difference between water
796 courses (derived from the drainage density per cell) and T the aquifer transmissivity obtained
797 from global hydrogeological datasets (e.g. Gleeson et al., 2014). A similar approach was used
798 by Cuthbert et al. (2019) to derive groundwater response times.

799
800 The drainable volume of groundwater stored in the groundwater reservoir ($\text{m}^3 \text{m}^{-2}$) of a grid
801 cell of a global hydrological model can also be expressed as: $V_g = n(h - h_s)$, with h_s the
802 surface water level and h the groundwater level in the cell. Substituting this into (B1) we
803 obtain the equivalent groundwater drainage equation for a grid cell:

$$804 \quad Q_g = \frac{n(h - h_s)}{J} \quad (\text{B3})$$

805
806 Comparing (B3) with (A2) shows that to obtain the same groundwater-surface water
807 exchange in the global hydrological model and the conceptual analytical model we must
808 have:

$$809 \quad C = \frac{J}{n} \quad (\text{B4})$$

810
811
812